Design and Optimization of the High Frequency Transformer for 100kW *CLLC* Converter

Zhe Zhao
Department of Electrical Engineering
University of Arkansas
Fayetteville, AR, USA
zhezhao@uark.edu

Yuheng Wu
Department of Electrical Engineering
University of Arkansas
Fayetteville, AR, USA
yuhengwu@uark.edu

Xinyuan Du
Department of Electrical Engineering
University of Arkansas
Fayetteville, AR, USA
xd006@uark.edu

Yue Zhao
Department of Electrical Engineering
University of Arkansas
Fayetteville, AR, USA
yuezhao@uark.edu

2021 IEEE Applied Power Electronics Conference and Exposition (APEC) | 978-1-7281-8949-9/21/$31.00 ©2021 IEEE | DOI: 10.1109/APEC42165.2021.9487200

***Abstract*—The *CLLC* converter is widely used in the power electronic applications as a DC transformer, which can provide galvanic isolation, bidirectional power flow and an adjustable output voltage with the use of proper controls. As the most critical component in the *CLLC* converter, the high frequency (HF) transformer should be optimized according to the design targets, such as efficiency and power density. Starting with the analysis of the *CLLC* operating characteristics, this paper proposes a formal approach to design the HF transformer of a 100kW *CLLC* converter for a grid-tied application. The optimization method for the HF transformer is presented and the effect of the resonant inductor is analyzed. The optimized transformer is simulated with the finite element analysis (FEA) and Matlab/Simulink.**

Keywords—CLLC converter, grid-tied converter, high frequency transformer

I. INTRODUCTION

The bidirectional *CLLC* resonant converter [1] is an attractive solution for the isolated DC power transfer. Their ability to achieve the zero-voltage-switching (ZVS) or zero-current-switching (ZCS) can nearly eliminate the switching losses, such that the use of high switching frequency is feasible. The ability of adjusting voltage by the frequency control is one main advantage of the *CLLC* converter. In addition, the high frequency (HF) transformer of the converter has a much lower volume than the traditional line frequency transformer, which can increase the converter power density [2]. Compared with the dual active bridge (DAB), which can also realize bidirectional power flow, the *CLLC* converter owns a wider range of soft switching. There exists extensive literature on the design and control of the *CLLC* converter [3], and it is proved that the *CLLC* converter can be utilized in high power applications with high efficiency and high power density [4]. With the development of advanced semiconductor devices [5] and the rapid growth of renewable energy [6], the *CLLC* converter can play an important role.

The magnetics, including inductors and transformers are indispensable parts in the power converters [7]. The HF transformer in the DC/DC converter has been extensively studied especially since the concept of solid-state transformer was proposed [8]. With the high operating frequency, the size and weight of the core can be reduced significantly. A recent trend is to bring the high frequency transformer into high power applications. However, a few problems occur in this case with efficiency optimization, thermal design and so on. Some research focused on the topic, and thus new models and optimization methods are introduced for accurate design of the transformer [9]. A 100kW, 10kHz transformer was built for series resonant converter (SRC) in [10], with accurate leakage inductance and thermal model. A developed genetic algorithm is used to optimize a 200kVA, 10kHz transformer for DAB with nanocrystalline core in [11]. A 200kW, 15kHz transformer for DAB with high insulation capability was shown in [12]. By using vacuum pressure potting approach, a 25kW, 48kHz transformer for SRC is presented in [13]. A water-cooled 166kW, 20kHz transformer for a multilevel SRC was obtained in [14]. However, the design of transformer for the high power, high current *CLLC* converter with sufficient ability of adjusting voltage is still lacking. A discussion about more details in the optimization of the HF transformer is needed.

In this paper, a grid-tied converter system from PV panel or battery energy storage to the 480V grid is studied, where the *CLLC* converter is used as a DC transformer. The HF transformer in the converter is focused and analyzed based on the parameters of the system. The design and optimization of the transformer is presented with proper loss and thermal model. The parameters of resonant tank are also optimized with considering the tradeoff between efficiency and power density. The operating properties of the optimal design is simulated and proved by FEA and Matlab/Simulink.

II. OPERATION PRINCIPLE OF THE *CLLC* CONVERTER

The topology of the entire converter system is shown in Fig. 1. The *CLLC* converter, the three-phase inverter and the *LCL* filter are combined to deliver the power from the PV panel to the grid. The PV panel generates 500 ~ 1000V input voltage and the full power level is 100kW. The output AC voltage is 480V L-L, which is commonly used in the industrial enviroment. The DC-link, which is formed with large capacitors, is used to reduce the variation of the DC voltage.

The typical topology of the *CLLC* converter is shown in Fig. 2, where L_m, L_{r1} and L_{r2} are the magnetizing inductance of the transformer, resonant inductors of the primary and secondary winding, respectively. The resonant capacitors, C_{r1} and C_{r2}, form the resonant tank with the aforementioned inductors. The turns-ratio of the transformer is n:1 and the total voltage gain of the converter can be expressed as

This work was supported in part by the U.S. National Science Foundation (NSF) within the Industry/University Cooperative Research Center (I/UCRC) on Grid Connected Advanced Power Electronic Systems (GRAPES) under Grant 1939144.

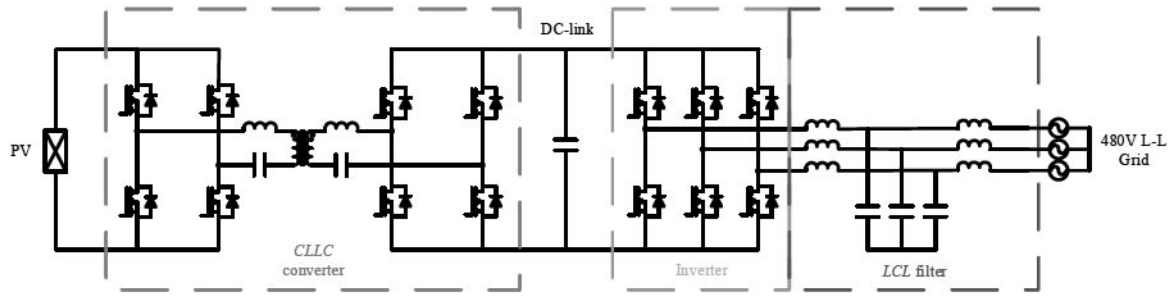

Fig. 1. The topology of the entire grid tied inverter system.

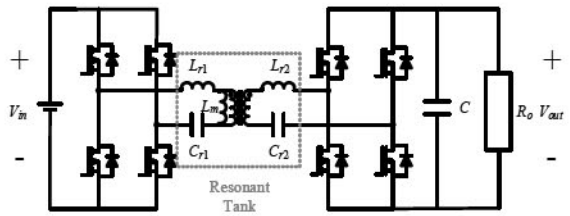

Fig. 2. The topology of the *CLLC* converter.

$$\|H_c\| = \frac{V_o}{V_{in}} = \|H_r\|/n \tag{1}$$

where $\|H_r\|$ is the voltage gain of the resonant tank, which is a function of the switching frequency f_s. To satisfy the input voltage range $V_{in,\min} \sim V_{in,\max}$ and output voltage range $V_{o,\min} \sim V_{o,\max}$, the required voltage gain of the converter in the operation range of $f_{s,\min} \sim f_{s,\max}$ should satisfy

$$\frac{V_{o,\min}}{V_{in,\max}} \le \|H_c\| \le \frac{V_{o,\max}}{V_{in,\min}} \tag{2}$$

The detailed operating principles of the *CLLC* converter can be found in [1]. The ZVS can be guaranteed if

$$L_m \le \frac{t_{dt}}{16 C_s f_{s,\max}} \tag{3}$$

where t_{dt} is the dead-time and C_s is the parasitic capacitance of the switches. The first harmonic approximation (FHA) is adopted to analyze the control model and the transfer function is derived as

$$\|H_c\| = \frac{Z_{eq}}{Z_{eq} + sL_{r1} + \dfrac{1}{sC_{r1}}} \cdot \frac{R_{oe}}{R_{oe} + sL_{r2e} + \dfrac{1}{sC_{r2e}}} \tag{4}$$

where L_{r2e}, C_{r2e}, R_{oe} and Z_{eq} can be calculated as

$$L_{r2e} = n^2 L_{r2} \tag{5}$$

$$C_{r2e} = C_{r2}/n^2 \tag{6}$$

$$R_{oe} = n^2 \frac{8}{\pi^2} R_o \tag{7}$$

$$Z_{eq} = \frac{sL_m\left(R_{oe} + sL_{r2e} + \dfrac{1}{sC_{r2e}}\right)}{R_{oe} + s\left(L_m + L_{r2e}\right) + \dfrac{1}{sC_{r2e}}} \tag{8}$$

Based on the transfer function, the typical bode diagram is shown in Fig. 3, where the f_m and f_r are the low and series resonant frequency, respectively. There exist two cases in the bode diagram: The gain curve is monotonic decreasing in the range of $f_m \sim f_r$ (Case I) when the inequality (46) in [1] is satisfied, which limits the ratio of the magnetizing inductance and resonant inductance, otherwise it becomes to Case II, where the range $f_m \sim f_r$ cannot be used for adjusting voltage. In Case II, the available operation range is reduced and only the turns-ratio of the transformer can increase the voltage, which means the available peak gain is equal to n. With the above discussion, the HF transformer for the *CLLC* converter can be designed.

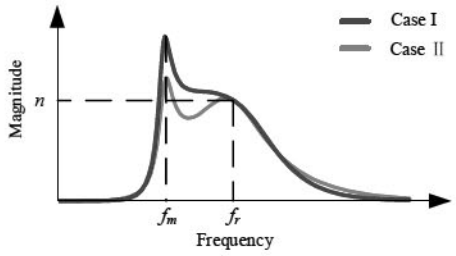

Fig. 3. The bode diagram of the *CLLC* converter. The difference between Case I and Case II is the existence of monotonicity between f_m and f_r.

III. Optimization of the HF Transformer at the Resonant Mode

To achieve an optimal design, some necessary parameters should be determined first. Then the loss and thermal model can be established and the optimization can be achieved with proper algorithm.

A. Basic Parameters

The output voltage of the *CLLC* converter, or the DC bus voltage, V_o, is a variable. On one hand, considering the 1700V SiC mosfets are selected as the switches, the maximum value of V_o is set as 1300V to ensure the safety of the devices. On the other hand, with the space vector pulse width modulation (SVPWM), which can increase the peak modulation ratio to $2/\sqrt{3}$, the minimum value of V_o is calculated as $480\sqrt{2}/\left(2/\sqrt{3}\right)\text{V} \approx 800\text{V}$ to provide enough voltage for the inverter. To reduce the pressure on the adjusting voltage for the *CLLC* converter, a variable DC-link is selected, i.e., the V_o varies from 800V to 1300V with the input voltage. Even though the ideal operation mode of the converter should be Case I, Case II is selected since it is hard to find a proper value of resonant inductor to satisfy the gain-curve-monotonically-decrease condition based on the parameters of the mosfets.

Since the efficiency of resonant converter reaches peak when it is operating in the resonant mode, the turns-ratio of the transformer n should be designed to make the range of operating in resonant mode as large as possible. In this case, the optimal value of n is

$$n = \frac{V_{o,\min}}{V_{in,\min}} = \frac{800\text{V}}{500\text{V}} = 1.6 \tag{9}$$

Noting that the numbers of turns of primary and secondary windings are integers, n can be a number around 1.6, and the maximum input voltage to operate in the resonant mode is

$$V_{in,res,\max} = \frac{V_{o,\max}}{n} = \frac{1300\text{V}}{1.6} \approx 800\text{V} \tag{10}$$

Thus, when the input voltage is from 500V to 800V, the *CLLC* converter will operate at resonant mode with high efficiency, otherwise the converter will operate at non-resonant mode, and thus the relationship of input voltage and output voltage is ploted in Fig. 4. This is a reasonable plan since the PV mostly operates with the low voltage [15], and thus the following optimization will be focusing on the V_{in} = 800V, $n \approx 1.6$ case.

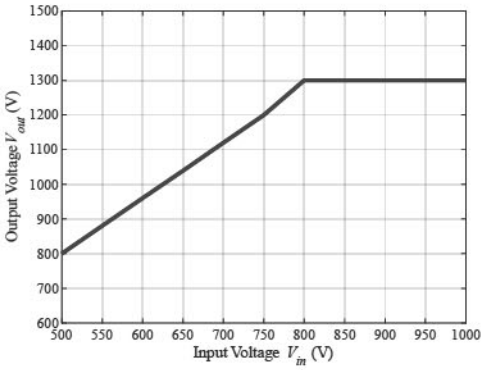

Fig. 4. The plot of input voltage and output voltage.

Another important parameter is the winding current. The rms value of primary winding current I_p can be obtained as

$$I_{p,rms} = \frac{nV_o}{2\sqrt{2}}\sqrt{\left(\frac{1}{2L_m f_s}\right)^2 + \left(\frac{\pi}{n^2 R_o}\right)^2} \tag{11}$$

For this converter, (11) can be simplified as

$$I_{p,rms} \approx \frac{nV_o}{2\sqrt{2}} \times \frac{\pi}{n^2 R_o} = \frac{\pi V_o}{2\sqrt{2} n R_o} \tag{12}$$

Assuming the power level is approximately proportional to the voltage for the PV panel,

$$P = kV_{in} \tag{13}$$

where k is the scale factor and equal to the ratio of the full power and full voltage

$$k = P_{max}/V_{in,\max} = 100\text{kW}/1000\text{V} = 0.1\text{kW/V} \tag{14}$$

And considering

$$R_o = \frac{V_o}{P} \tag{15}$$

Substituting (1), (13) - (15) into (12)

$$I_{p,\text{rms}} = \frac{111}{\|H_r\|} \tag{16}$$

where the rms value of primary winding current is inversely proportional to the voltage gain of the resonant tank. Since Case II of the *CLLC* converter is selected, the peak value of $\|H_r\|$ is unit which occurs at the resonant mode, and the corresponding value of $I_{p,\text{rms}}$ is 111A. As a result, expanding the range of operating in resonant mode can decrease the winding current and thus reduce the winding loss. When the converter is operating at full power, $\|H_r\|$ reaches its minimum value, and the peak value of $I_{p,\text{rms}}$ is calculated as 137A, which is a significant parameter for litz wire design to avoid overheat on the winding.

B. Loss Evaluation

The power loss of a transformer consists of both the core loss P_{Fe} and the winding loss P_{Cu}. For the core loss, the improved generalized Steinmetz equation (IGSE) is proved to have improved accuracy than the original Steinmetz equation especially for non-sinusoidal excitation [16]. Based on the square voltage waveform of the *CLLC* converter and the measured Steinmetz coefficients K, α and β, the IGSE can be expressed as

$$P_{Fe} = V_c \times 2^{2\alpha+\beta-1} k_i f_s^{\alpha} B_{\text{m}}^{\beta} \tag{17}$$

where V_c is the volume of the core, B_m is the maximum flux density, and k_i is given as

$$k_i = \frac{K}{(2\pi)^{\alpha-1}\int_0^{2\pi}\left|\cos\theta\right|^{\alpha} 2^{\beta-\alpha} d\theta} \tag{18}$$

At the frequency from 10kHz to 50kHz, nanocrystalline core material is proved to have lower core loss than the ferrite core [17], and thus selected for the optimization.

The winding loss is affected by the high frequency effects. The skin depth δ is a crucial parameter to represent the uneven distribution of current in conductors under high frequency electromagnetic field, and can be obtained as

$$\delta = \sqrt{\frac{\rho}{\pi \mu_0 f_s}} \tag{19}$$

where ρ is the conductor resistivity, and μ_0 is the free-space permeability. A classical calculation method for winding loss is proposed by Dowell [18] and based on this model, an optimal design of multi-strand litz wire is presented in [19]. Especially, for the square litz wire shown in Fig. 5, in which d is the strand diameter, k is the number of strands in a bundle,

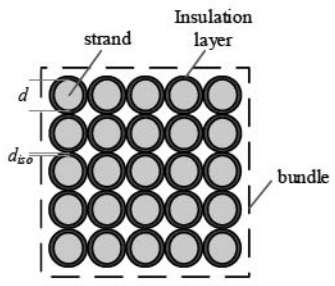

Fig. 5. The structure of square litz wire in a bundle.

and d_{iso} is the thickness of the isolation layer for each strand with the thickness of the layer in the same winding layer, an approximate equation of the ratio of AC winding loss and DC winding loss, F_R, is given as

$$F_R \approx 1+\frac{5m^2k-1}{45}\Delta^4 \tag{20}$$

where m is the number of layers, k is the number of strands in a bundle and Δ is expressed as

$$\Delta=\left(\frac{\pi}{4}\right)^{0.75}\frac{d}{\delta}\sqrt{\eta} \tag{21}$$

where η is the porosity factor and defined as

$$\eta=\frac{d}{d+2d_{iso}} \tag{22}$$

Then the total winding is calculated as

$$P_{Cu}=R_{dc}\sum_{n=1}^{\infty}I_n^2F_{Rn} \tag{23}$$

where R_{dc} is the dc resistance of the winding, I_n and F_{Rn} are the value of the winding current and F_R at the nth harmonic frequency range after fast Fourier transform (FFT), respectively. Based on (23), the optimal value of d to minimize the winding loss can be derived as [11]

$$d_{op}=\frac{M}{\sqrt{\eta}} \tag{24}$$

where M is given as

$$M=\frac{\delta}{\left(\frac{\pi}{4}\right)^{0.75}}\sqrt[4]{\frac{45}{5m^2k-1}\frac{\sum_{n=1}^{\infty}I_n^2}{\sum_{n=1}^{\infty}n^2I_n^2}} \tag{25}$$

However, (24) is unclear to calculate since η and k are also related with d. A complicated equation is obtained after substituting (22) and (25) into (24), and the equation can be solved with numerical computation. Then the corresponding optimal value of k is

$$k_{op}=\frac{I}{\frac{\pi}{4}d_{op}^2J} \tag{26}$$

where J is the current density in the winding. The plot of d_{op} verses frequency with the sinusoidal current varying from 50A to 150A at m = 1, J = 3A/mm^2 and d_{iso} = 0.005mm is shown in Fig. 6(a). Also, to illustrate the influence of m, Fig. 6(b) shows the plot of d_{op} verses frequency with m varies from 1 to 5 at I = 100A, J = 3A/mm^2 and d_{iso} = 0.005mm. It can be concluded that

- With the increase of the current, more strands in a bundle results in higher proximity effect, and strands with smaller diameter are needed.
- The larger number of layers m can worsen the winding losses, especially with the high winding current. The following optimization should reduce m as much as possible.

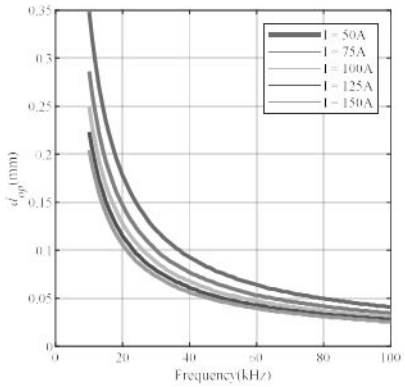

(a)

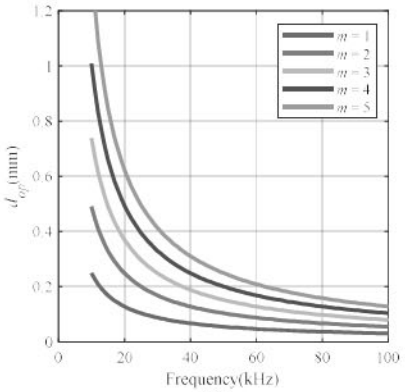

(b)

Fig. 6. The value of optimal strand diameter under different frequency with (a) variable current; (b) variable number of layers.

Loss model is significant for both the efficiency estimation and the thermal design. With the calculated core loss and winding loss data, the heat sources in the thermal model can be determined.

C. Thermal Model

For the transformer with high power density, the thermal dissipation can become a serious problem, thus an accurate thermal model should be set up for predicting the temperature distribution. Even though transient thermal model can be adopted to analyze dynamic performance analysis of the transformer [20], the simplified steady state model is used to reduce the computation. For the shell structure of transformer, which is commonly used for high power application, the thermal network shown is set up based on the method proposed in [10]. With the different kinds of area A, the thermal resistance can be calculated with the following equations for conduction, convection and radiation,

$$R_c=\frac{l}{\lambda A} \tag{27}$$

$$R_{conv}=\frac{1}{\alpha_{conv}A} \tag{28}$$

$$R_r=\frac{1}{\alpha_r A} \tag{29}$$

where l is the thickness of the pad in the thermal flow direction, λ is the thermal conductivity of the material, α_{conv} is the convective heat transfer coefficient, and α_r is the radiative heat transfer coefficient. α_{conv} and α_r can be calculated with the thermal parameters of the material and experiential formulas [21]. The temperature of core and windings can be obtained after solving the thermal network.

D. Pareto Optimization

To achieve high efficiency, high power density and avoid overheat of the transformer, the Pareto optimization [22] is used based on the above loss and thermal model. The off-the-shelf Hitachi FINEMET® FT-3L nanocrystalline C-cores are evaluated because of the high saturation flux density and low core loss [11]. The flow chart of optimization algorithm is shown in Fig. 7, where the resonant frequency is also set as a variable. The input variables can be written as

$$x = \left(x_{core}, x_{pw}, x_{sw}, f_s \right) \tag{30}$$

where x_{core} contains the size and the number of the cores, x_{pw} and x_{sw} contain the number of turns and current density for the primary and secondary windings, respectively. The output variables can be expressed as

$$y = \left(y_{litz}, \eta_{eff}, \sigma_{pd}, T \right) \tag{31}$$

where y_{litz} contains the parameters of litz wire, η_{eff} is the efficiency, σ_{pd} is the power density and T contains the peak temperature of core and winding. The constraints in the algorithm are summarized as Table I.

The optimization result is shown in Fig. 8, where the power density shown is for 80kW operation and its final value should time 1.25. The parameters of selected design are shown in Table II. The approximate sizes of square litz wire for the primary and secondary windings are 7.2×7.2mm and 5.8×5.8mm, respectively. The modified polyurethane (PU) is used for insulation between adjacent strands. The 3D model of the transformer is shown in Fig. 9.

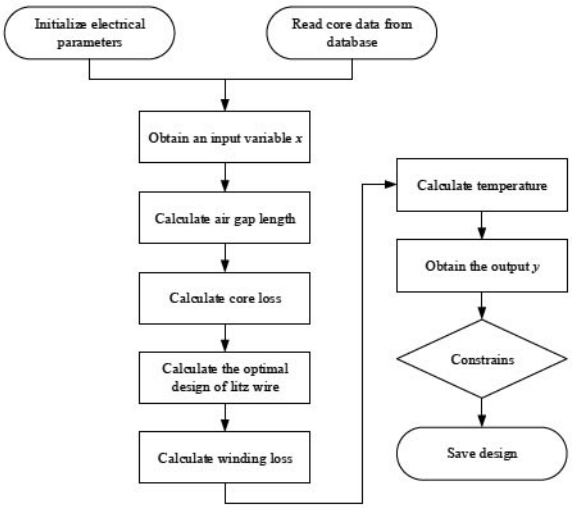

Fig. 7. The Pareto optimization algorithm. The calculation repeats for each new input variable x.

TABLE I. CONSTRAINTS FOR OPTIMIZATION

Parameters	Constraints
AWG of litz wire	⩽ 41
k	⩽ 5000
B_{max} (T)	⩽ 0.8
T_{core} (℃)	⩽ 100
$T_{winding}$ (℃)	⩽ 125

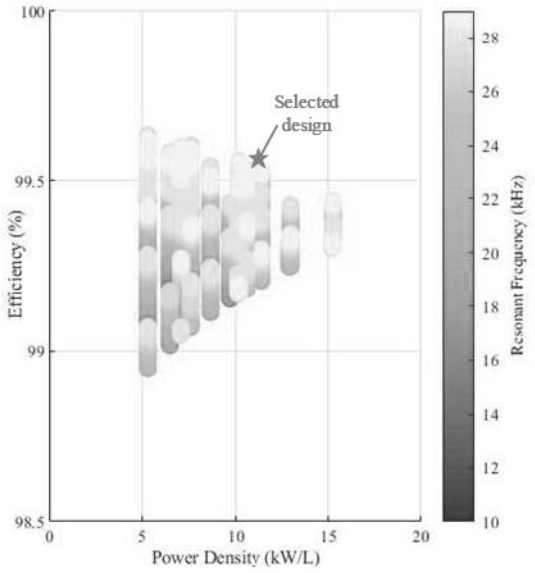

Fig. 8. Result of optimization at V_{in} = 800V, P = 80kW. The resonant frequency is also considered as a variable to get the optimal design.

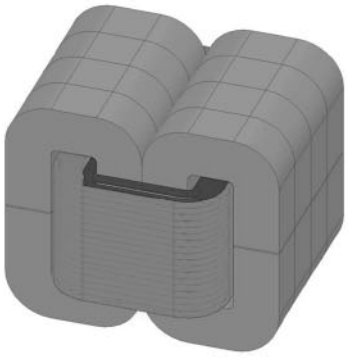

Fig. 9. The 3D model of the optimal design. The blue and red coils are the primary and secondary winding, respectively.

TABLE II. KEY PARAMETERS OF THE OPTIMAL TRANSFORMER

Parameters		Values
Cores		FINEMET® F1AH1267×8
Litz wire	Primary	AWG 39 × 4500
	Secondary	AWG 39 × 3140
Turns-ratio		11:18
Resonant frequency (kHz)		29
Power density (kW/L)	@ 80kW	11.5
	@ 100kW	14.3
Efficiency @ 80kW		99.55%

E. Design of Resonant Tank

The above optimization is focusing on the resonant mode and the effects of the resonant inductors are not considered. Based on the optimal design, the parameters of resonant tank should be determined. For full power operation, a larger value of maximum switching frequency $f_{s,max}$ is required with the increase of L_{r1}, and it can shrink the ZVS range and increase the winding loss. Considering the high winding current and high frequency operation of the converter, it is hard to produce the litz wire with both large number and small size of the strands, and thus a larger L_{r1} is preferred for higher efficiency operation. An ideal solution is to use the leakage inductor $L_{leakage}$ of the transformer as the resonant inductor, and one reasonable opinion is adjusting the position of the windings to obtain the required total leakage inductance [11], [23]. However, for the *CLLC* converter, it is the leakage inductance of the primary and secondary winding, $L_{leakage1}$ and $L_{leakage2}$, rather than $L_{leakage}$ is needed to design since both of the leakage inductors participate in the resonant process individually, and it increases the difficulty of the design. Especially, it is hard to determine $L_{leakage1}$ and $L_{leakage2}$ together with mathematical calculation for the transformer with non-unity turns-ratio, and thus auxiliary inductor is required. However, a large-sized auxiliary inductor is required to achieve the large L_{r1}, and it can decrease the power density of the whole converter. To determine the parameters of the resonant tank, the plot of switching frequency and efficiency verses L_{r1} under full power operation is shown in Fig. 10. 6μH is set as the optimal value of L_{r1} since the improvement of efficiency becomes non-obvious after L_{r1} increases to 6μH. Then the parameters of the resonant tank can be determined as L_{r1} = 6μH, L_{r2} = 16μH, C_{r1} = 5μF and C_{r2} = 1.86μF.

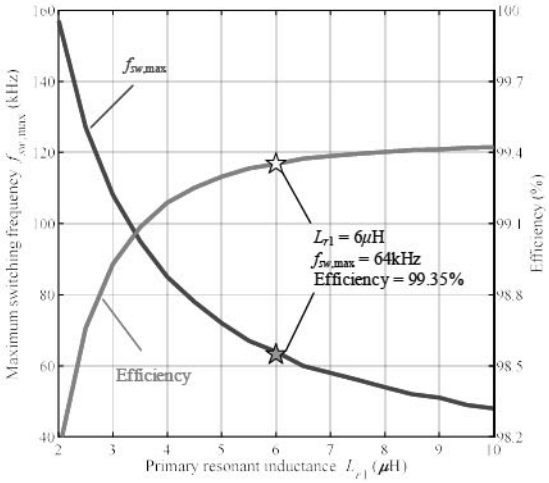

Fig. 10. The effect of resonant inductance on the switching frequency and efficiency at the full power. 6μH is the selected value for L_{r1}.

With the optimal design of resonant tank, the plots of the switching frequency and efficiency in the full operation range are both shown in Fig. 11. When the power level P exceeds 80kW, the operation of the converter transfers from resonant mode to non-resonant mode, and thus the efficiency is reduced. The peak efficiency is 99.57% and the full power efficiency is 99.35%.

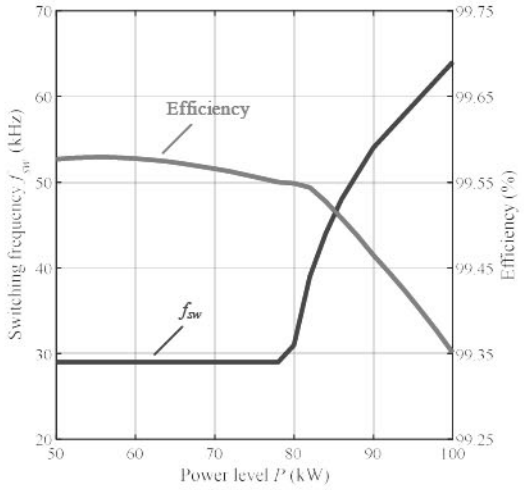

Fig. 11. The switching frequency and efficiency curves in the whole operation range. The former varies from 29kHz to 64kHz, and the latter varies from 99.57% to 99.35%.

IV. SIMULATION AND ANALYSIS

A. Insulation and Thermal Analysis

For the dry-type transformer, the required dielectric insulation level with different voltage level is shown in [24]. To ensure the reliability of the high frequency transformer, the electric field distribution is simulated by ANSYS/Maxwell. A 10kV voltage is applied between the two windings, and from the FEA result shown in Fig. 12, it can be seen that the maximum electric field strength is 8.45kV/mm, which is much lower than the dielectric strength of the insulation components shown in Table. III.

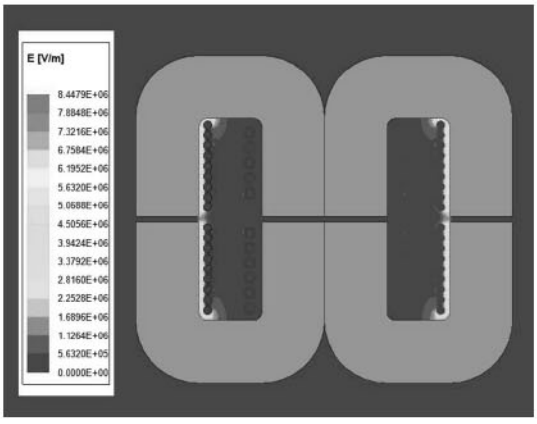

Fig. 12. The electric field distribution of the transformer from FEA. The positions of high electric field strength are concentrated around the high voltage winding.

TABLE III. DIELECTRIC STRENGTH OF INSULATION COMPONENTS

Component	Material	Dielectric Strength (kV/mm)
Bobbin	Epoxy resin	20.8
125μm Kapton® Type HN	Polyimide	154

Under natural convection, the temperature distribution of the transformer at full power is simulated by ANSYS/Icepak and the result is shown in Fig. 13. In both of the core and windings, the temperature of bottom part is higher since the existence of gravity. The peak temperature of the transformer occurs at the primary winding, which is arranged close to the core. The compact structure increases the thermal coupling between the core and the primary winding.

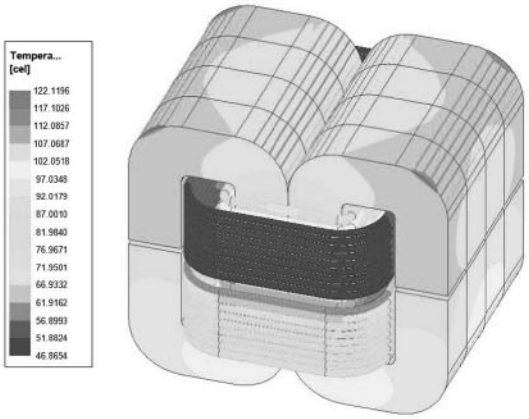

Fig. 13. The simulated temperature distribution of the transformer. The hot spots are on the primary winding.

B. *Voltage and Current of the System*

With the optimal design of the high frequency transformer, the simulation studies of the *CLLC* converter are performed in Matlab/Simulink. Fig. 14(a) and (b) shows the simulated waveforms of output voltage and winding current for 80kW and 100kW operation, respectively. For the former case, the converter is operating in the resonant mode, and the winding current is approximately sinusoidal. For the latter case, the non-resonant operation mode distorts the current waveform, and both the peak value and rms value of the current increase with the higher power level. It is noted that with 64kHz switching frequency, the output voltage of the latter cases only reaches to 1170V, which is 10% lower than the required 1300V. The error comes from the FHA since the effect of harmonics beyond fundamental frequency is neglected. In practical operation, the accuracy can be improved by applicable control methods. The adjusted switching frequency is 57kHz, and the corresponding output voltage is 1260V with only 3% error as shown in Fig. 14(c). The above results prove that the *CLLC* converter can operate well and provide required DC voltage to the following DC link and three-phase inverter.

V. CONCLUSIONS AND FUTURE WORK

In this work, the design and optimization of a high frequency transformer for a 100kW *CLLC* converter in the PV application is presented. Based on the structure of the PV system and the operation principle of the *CLLC* converter, some parameters of the transformer are determined first for large ability of adjusting voltage and high efficiency operation, and rest of the parameters are optimized by the adoption of proper models and Pareto optimization algorithm. The effect of the resonant inductance is analyzed, and with the designed resonant tank, the efficiency of the transformer in the whole operation range is obtained, and the peak efficiency reaches 99.57%. At full load operation, the power density of the transformer exceeds 14kW/L.

The insulation and thermal designs of the transformer are completed and verified by FEA, and the operation properties of the *CLLC* converter are simulated by Matlab/Simulink. In the future, the prototype of the optimal design will be built, and experimental results will be presented.

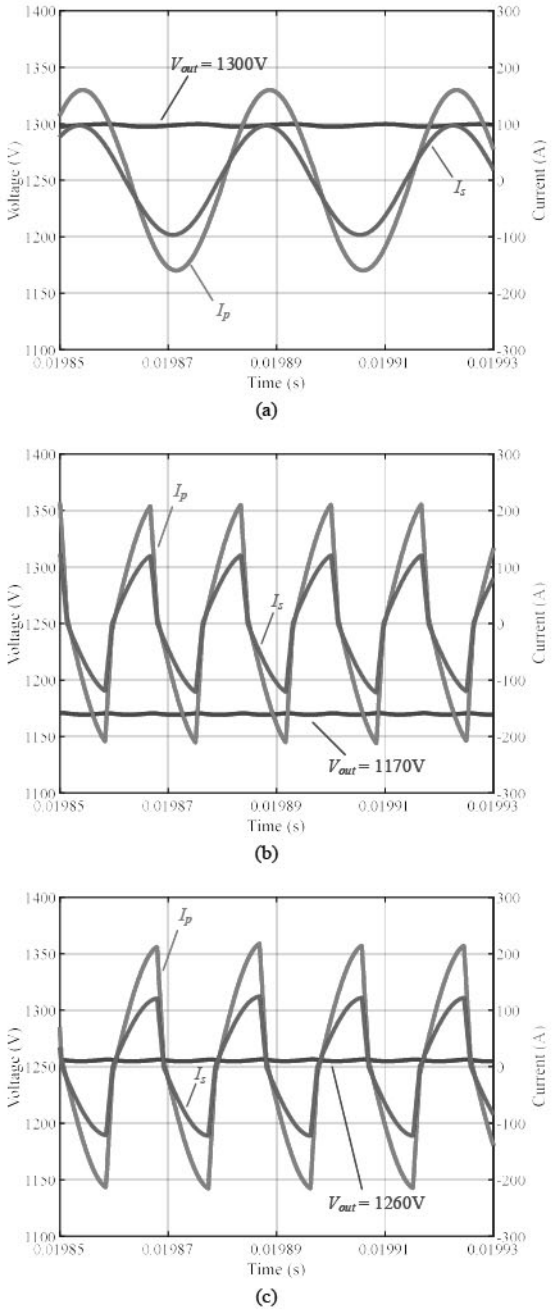

Fig. 14. The simulated waveforms for output voltage and winding current of the *CLLC* converter at (a) resonant mode; full power (b) with switching frequency calculated by FHA and (c) with adjusted switching frequency.

REFERENCES

[1] J. Jung, H. Kim, M. Ryu, and J. Baek, "Design Methodology of Bidirectional CLLC Resonant Converter for High-Frequency Isolation

of DC Distribution Systems," in *IEEE Transactions on Power Electronics*, vol. 28, no. 4, pp. 1741-1755, April 2013.

[2] D. Dong, M. Agamy, J. Z. Bebic, Q. Chen, and G. Mandrusiak, "A Modular SiC High-Frequency Solid-State Transformer for Medium-Voltage Applications: Design, Implementation, and Testing," in *IEEE Journal of Emerging and Selected Topics in Power Electronics*, vol. 7, no. 2, pp. 768-778, June 2019.

[3] J. Huang, X. Zhang, A. Zhang, and P. Wang, "Comprehensive Coordinated Frequency Control of Symmetrical CLLC-DC Transformer in Hybrid AC/DC Microgrids," in *IEEE Transactions on Power Electronics*, vol. 35, no. 10, pp. 10374-10384, Oct. 2020.

[4] B. Li, Q. Li, and F. C. Lee, "High-Frequency PCB Winding Transformer with Integrated Inductors for a Bi-Directional Resonant Converter," in *IEEE Transactions on Power Electronics*, vol. 34, no. 7, pp. 6123-6135, July 2019.

[5] Z. Wang et al., "Design and Validation of A 250-kW All-Silicon Carbide High-Density Three-Level T-Type Inverter," in *IEEE Journal of Emerging and Selected Topics in Power Electronics*, vol. 8, no. 1, pp. 578-588, March 2020.

[6] T. Mai et al., "Renewable Electricity Futures for the United States," in *IEEE Transactions on Sustainable Energy*, vol. 5, no. 2, pp. 372-378, April 2014.

[7] Z. Zhao, F. Diao, Y. Wu, N. Lin, and Y. Zhao, "An Inductor Current Estimation Approach for DC/DC Converters Based on Bisection Method," *2020 IEEE Energy Conversion Congress and Exposition (ECCE)*, Detroit, MI, USA, 2020, pp. 3215-3219.

[8] X. She, A. Q. Huang, and R. Burgos, "Review of solid-state transformer technologies and their application in power distribution systems," *IEEE J. Emerg. Sel. Topics Power Electron.*, vol. 1, no. 3, pp. 186–198, Sep. 2013.

[9] G. Zhu et al., "Wireless Power Transformation for Data Centers and Medium Voltage Applications," 2020 *IEEE Applied Power Electronics Conference and Exposition (APEC)*, New Orleans, LA, USA, 2020, pp. 798-804.

[10] M. Mogorovic and D. Dujic, "100 kW, 10 kHz Medium-Frequency Transformer Design Optimization and Experimental Verification," in *IEEE Transactions on Power Electronics*, vol. 34, no. 2, pp. 1696-1708, Feb. 2019.

[11] B. Chen, X. Liang, and N. Wan, "Design Methodology for Inductor-Integrated Litz-Wired High-Power Medium-Frequency Transformer with the Nanocrystalline Core Material for Isolated DC-Link Stage of Solid-State Transformer," in *IEEE Transactions on Power Electronics*, vol. 35, no. 11, pp. 11557-11573, Nov. 2020.

[12] Z. Guo, S. Sen, S. Rajendran, Q. Huang, X. Feng, and A. Q. Huang, "Design of a 200 kW Medium-Frequency Transformer (MFT) With High Insulation Capability," *2020 IEEE Energy Conversion Congress and Exposition (ECCE)*, Detroit, MI, USA, 2020, pp. 3471-3477.

[13] D. Rothmund, T. Guillod, D. Bortis, and J. W. Kolar, "99% Efficient 10 kV SiC-Based 7 kV/400 V DC Transformer for Future Data Centers," in *IEEE Journal of Emerging and Selected Topics in Power Electronics*, vol. 7, no. 2, pp. 753-767, June 2019.

[14] M. Leibl, G. Ortiz, and J. W. Kolar, "Design and Experimental Analysis of a Medium-Frequency Transformer for Solid-State Transformer Applications," in *IEEE Journal of Emerging and Selected Topics in Power Electronics*, vol. 5, no. 1, pp. 110-123, March 2017.

[15] N. Femia, G. Petrone, G. Spagnuolo, and M. Vitelli, "Optimization of perturb and observe maximum power point tracking method," in *IEEE Transactions on Power Electronics*, vol. 20, no. 4, pp. 963-973, July 2005.

[16] K. Venkatachalam, C. R. Sullivan, T. Abdallah and H. Tacca, "Accurate prediction of ferrite core loss with nonsinusoidal waveforms using only Steinmetz parameters," *2002 IEEE Workshop on Computers in Power Electronics, 2002. Proceedings.*, Mayaguez, PR, USA, 2002, pp. 36-41.

[17] W. Shen, F. Wang, D. Boroyevich, and C. W. Tipton IV, "High-Density Nanocrystalline Core Transformer for High-Power High-Frequency Resonant Converter," in *IEEE Transactions on Industry Applications*, vol. 44, no. 1, pp. 213-222, Jan.-feb. 2008.

[18] P. L. Dowell, "Effects of eddy currents in transformer windings." *Proceedings of the Institution of electrical Engineers*, vol. 113, no. 8, IET Digital Library, 1966.

[19] R. P. Wojda and M. K. Kazimierczuk, "Winding resistance of litz-wire and multi-strand inductors," in *IET Power Electronics*, vol. 5, no. 2, pp. 257-268, Feb. 2012.

[20] A. K. Das et al., "Thermal modeling and transient behavior analysis of a medium-frequency high-power transformer," *IECON 2017 - 43rd Annual Conference of the IEEE Industrial Electronics Society*, Beijing, China, 2017, pp. 2213-2218.

[21] Bergman, Theodore L., et al. *Fundamentals of heat and mass transfer*. John Wiley & Sons, 2011.

[22] R. Bosshard et al., "Modeling and η - α -Pareto Optimization of Inductive Power Transfer Coils for Electric Vehicles," in *IEEE Journal of Emerging and Selected Topics in Power Electronics*, vol. 3, no. 1, pp. 50-64, March 2015.

[23] T. Jimichi, M. Kaymak, and R. W. De Doncker, "Design and Experimental Verification of a Three-Phase Dual-Active Bridge Converter for Offshore Wind Turbines," *2018 International Power Electronics Conference (IPEC-Niigata 2018 -ECCE Asia)*, Niigata, Japan, 2018, pp. 3729-3733.

[24] "IEEE Standard for General Requirements for Dry-Type Distribution and Power Transformers," in *IEEE Std C57.12.01-2020 (Revision of IEEE Std C57.12.01-2015)*, vol., no., pp.1-49, 24 Nov. 2020.